Xiao et al. *Zool. Res.* 2024, 45(1): 55−68
https://doi.org/10.24272/j.issn.2095-8137.2023.007

ZR | Zoological Research

Article Open Access

Single-cell profiling of the pig cecum at various developmental stages

Yan-Yuan Xiao[1], Qing Zhang[1], Fei Huang[1], Lin Rao[1], Tian-Xiong Yao[1], Si-Yu Yang[1], Lei Xie[1], Xiao-Xiao Zou[1], Li-Ping Cai[1], Jia-Wen Yang[1], Bin Yang[1,*], Lu-Sheng Huang[1,*]

[1] *National Key Laboratory for Swine Genetic Improvement and Germplasm Innovation*, *Ministry of Science and Technology of China*, *Jiangxi Agricultural University*, *Nanchang*, *Jiangxi* 330045, *China*

ABSTRACT

The gastrointestinal tract is essential for food digestion, nutrient absorption, waste elimination, and microbial defense. Single-cell transcriptome profiling of the intestinal tract has greatly enriched our understanding of cellular diversity, functional heterogeneity, and their importance in intestinal tract development and disease. Although such profiling has been extensively conducted in humans and mice, the single-cell gene expression landscape of the pig cecum remains unexplored. Here, single-cell RNA sequencing was performed on 45 572 cells obtained from seven cecal samples in pigs at four different developmental stages (days (D) 30, 42, 150, and 730). Analysis revealed 12 major cell types and 38 subtypes, as well as their distinctive genes, transcription factors, and regulons, many of which were conserved in humans. An increase in the relative proportions of $CD8^+$ T and Granzyme A (low expression) natural killer T cells ($GZMA^{low}$ NKT) cells and a decrease in the relative proportions of epithelial stem cells, Tregs, $RHEX^+$ T cells, and plasmacytoid dendritic cells (pDCs) were noted across the developmental stages. Moreover, the post-weaning period exhibited an up-regulation in mitochondrial genes, *COX2* and *ND2* , as well as genes involved in immune activation in multiple cell types. Cell-cell crosstalk analysis indicated that $IBP6^+$ fibroblasts were the main signal senders at D30, whereas $IBP6^-$ fibroblasts assumed this role at the other stages. NKT cells established interactions with epithelial cells and $IBP6^+$ fibroblasts in the D730 cecum through mediation of *GZMA-F2RL1/F2RL2* pairs. This study provides valuable insights into cellular heterogeneity and function in the pig cecum at different development stages.

Keywords: Single-cell RNA-seq; Cecum; Bama Xiang pigs; Various developmental stages; Cellular heterogeneity

INTRODUCTION

Pigs are one of the most important farm animals, providing approximately 40% of global red meat consumption (Gerrits et al., 2005). Additionally, they are valuable biomedical models due to their anatomical, structural, immunological, physiological, and genomic similarities to humans (Lunney et al., 2021). The gastrointestinal tract, essential for food digestion and waste expulsion (Liao et al., 2009; Zorn & Wells, 2009), is also the largest immune organ in the body, accommodating trillions of microorganisms (Chassaing et al., 2014; James, 1993). The cecum, a pouch or large tubelike structure situated immediately after the ileocecal junction, demarcates the transition from the small to large intestine. Lying between the non-fermentative and fermentative parts of the gut, the cecum serves as a fermentation chamber, facilitating the conversion of indigestible fibers into energy-rich compounds (Stumpff et al., 2019) and plays an important role in electrolyte and water absorption (Dabareiner & White II, 1997). Cecum removal has been shown to severely affect short-chain fatty acid production and reduce resistance to *Salmonella enterica* serovar Enteritidis infection in mice (Brown et al., 2018). Proper gut functionality requires the cooperation of multiple cell lineages. Single-cell RNA sequencing (scRNA-seq) has enabled detailed gene expression profiling of tissues and organs at the single-cell level (Han et al., 2018, 2020, 2022; Li et al., 2022). Notably, scRNA-seq has been extensively applied in human and mouse studies to profile the intestinal tract (Elmentaite et al., 2021; Fawkner- Corbett et al., 2021; Wang et al., 2020), shedding light on cell types and genes associated with intestinal tract development and diseases. However, a comprehensive examination of the single-cell gene expression profiles of the pig cecum is yet to be conducted.

The weaning process represents an important stage in pig farming. During weaning, piglets transition from a diet of highly

Received: 16 March 2023; Accepted: 12 September 2023; Online: 13 September 2023

Foundation items: This work was supported by the National Natural Science Foundation of China (31790410, 32160781)

*Corresponding authors, E-mail: binyang@live.cn; lushenghuang@hotmail.com

digestible and palatable liquid milk to less digestible and palatable solid dry feed (Campbell et al., 2013). This abrupt dietary shift can induce weaning stress, potentially leading to intestinal dysfunction, reduced growth, compromised health, and reduced feed intake, particularly during the first week of weaning (Campbell et al., 2013; Tang et al., 2022). However, what effects the weaning process has on the gut at the single-cell level remain poorly understood.

In this study, scRNA-seq was conducted on seven cecal samples obtained from pigs aged 30, 42, 150, and 730 days, yielding 45 572 cells after quality control. We identified a total of 12 major cell types and 38 subtypes, including major intestinal epithelial cells, such as goblet cells, enterocytes, and stem cells, and various lymphocyte and myeloid immune cell lineages, and characterized cell-type-specific marker genes, transcription factors (TFs), and regulons. We observed substantial cellular heterogeneity in the cecum across the four developmental stages and identified dynamic changes in gene expression in different cell types during weaning. Furthermore, we also revealed cell-cell interaction heterogeneity across the different developmental stages, as well as cell-type conservation in cecal tissue between pigs and humans. These findings enhance our understandings of cellular diversity across different developmental stages in the pig cecum.

MATERIALS AND METHODS

Pig cecal tissue collection and ethics statement

Cecal samples were obtained from seven healthy Bama Xiang pigs at four different developmental stages: D30 (30 days after birth, five days before weaning), D42 (42 days after birth, seven days after weaning), D150 (150 days after birth), and D730 (730 days after birth). The cecal samples were collected from one boar at D150 and from three pairs of full siblings (both sexes) at the other three developmental stages, with a single sample per individual (Supplementary Table S1). All samples were consistently harvested from the bottom region

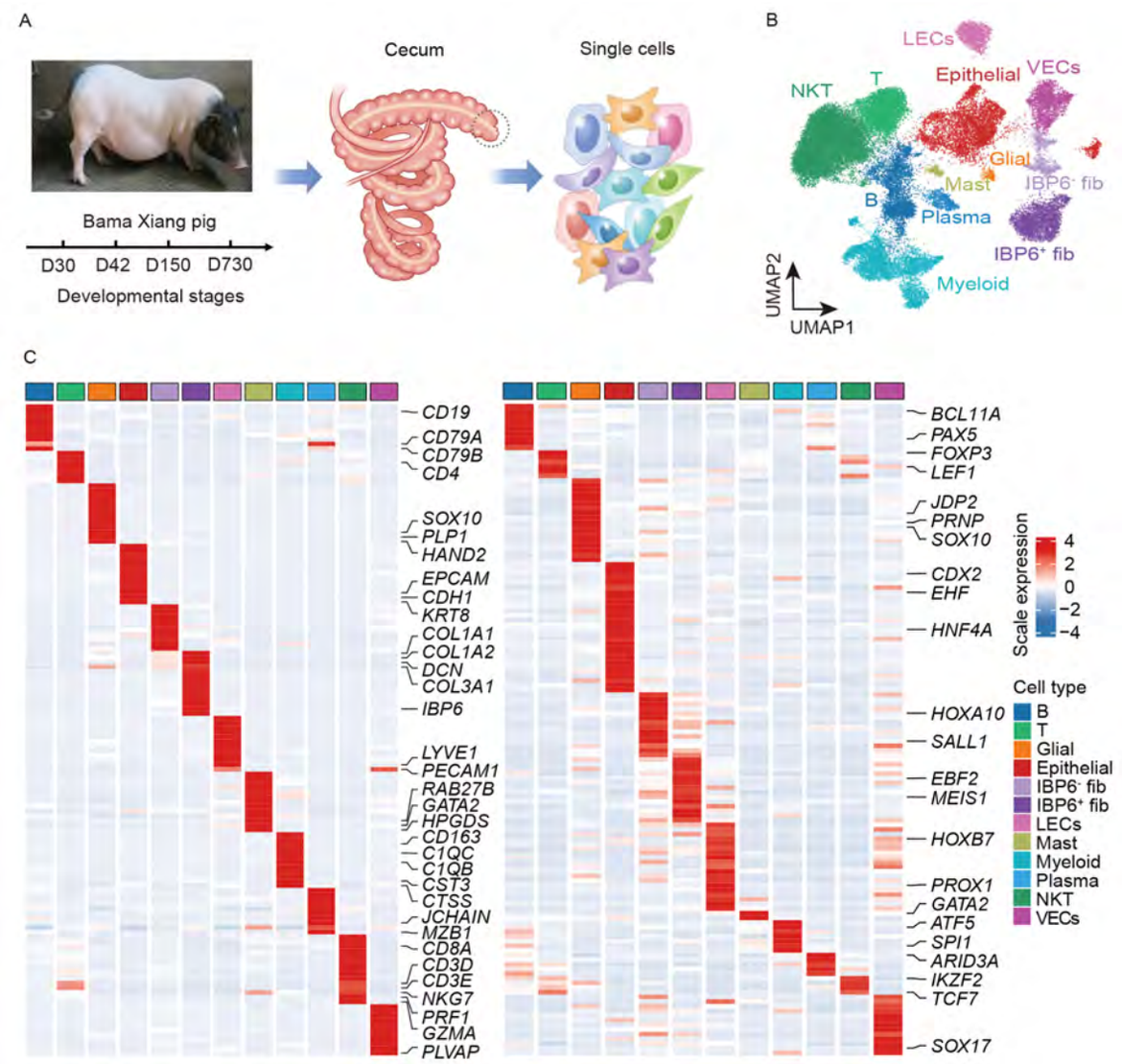

Figure 1 ScRNA-seq profiling of pig cecum at four developmental stages

A: Experimental schematic. Circled section in middle figure is the specific sampling site. D30: 30 days after birth (five days before weaning); D42: 42 days after birth (seven days after weaning); D150: 150 days after birth; D730: 730 days after birth. B: UMAP of 45 572 cells colored by major cell types. B: B cells, T: T cells, Glial: enteric glial cells, Epithelial: epithelial cells, IBP6$^-$ fib: IBP6$^-$ fibroblasts; IBP6$^+$ fib: IBP6$^+$ fibroblasts; LECs: lymphatic endothelial cells, Mast: mast cells, Myeloid: myeloid cells, Plasma: plasma cells, NKT: natural killer T cells, VECs: vascular endothelial cells. C: Heatmap showing highly expressed genes in cell types (left) and cell-type-specific TFs (right).

of the cecum (Figure 1A). Pigs were fed their mother's milk before weaning (D30), then a solid dry feed diet (corn-soyabean-based diet composed of 15%–18% crude protein, ≥ 1.05% lysine, 0.40%–1.20% calcium, and ≥0.40% phosphorus) after weaning. All animal experiments were approved by the Animal Ethics Committee of Jiangxi Agricultural University.

Cell suspension for scRNA-seq

Cecal tissue was harvested and washed in ice-cold RPMI 1640. Tissue slices (0.4 mm^2) were then dissociated using a Multi-Tissue Dissociation Kit 2 (Miltenyi Biotec, Germany) as per the manufacturer's instructions. After DNase treatment, fresh cells were washed twice in RPMI 1640 and resuspended at 1×10^6 cells/mL in 1×phosphate buffered saline (PBS) and 0.04% bovine serum albumin.

Library construction and sequencing

ScRNA-seq libraries were prepared using a SeekOne® MM Single-Cell 3' Library Preparation Kit. The PE150 libraries were sequenced using the Illumina NovaSeq 6000 platform (USA).

ScRNA-seq data analysis

The raw scRNA-seq reads were first trimmed using Fastp (v.0.20.1) (Chen et al., 2018) to obtain clean reads. The specific parameters were: --cut_front --cut_front_Window_size 4 -- cut_front_mean_quality 10, --cut_tail --cut_tail_window_size 1 -- cut_tail_mean_quality 3, detect_adapter_for_pe, --length_required 60. The obtained clean reads were processed using the Seekone Tools pipeline (https://www.seekgene.com/fxrj) to generate a transcript expression matrix. A counting matrix was then imported into the Python package Scanpy (v.1.7.1). Quality control procedures were performed on each sample: (1) removal of genes expressed in fewer than three cells and (2) exclusion of cells containing less than 300–450 genes, more than 2 500–4 000 genes, more than 13 000–20 000 unique molecular identifier (UMI) counts, or mitochondrial read fraction of more than 40%–45%. Furthermore, doublet exclusion was performed using Scrublet (v.0.2.3) with a cut-off score of 0.25 and expected doublet rate of 0.0225–0.0445 depending on the number of captured cells.

Library size was normalized and the effects of UMI counts and percentage of mitochondrial reads on gene expression were regressed out. Batch corrections of the seven cecal samples were performed using Harmony (Korsunsky et al., 2019). Dimensionality reduction and Louvain clustering using the top 2 000 highly variable genes were carried out with default parameters. Differential expression analysis was performed using the *sc.tl.rank_genes_groups* (method= "Wilcoxon") function in Scanpy.

Cell-type-specific TFs

The list of TFs was downloaded from the SCENIC GitHub repository (Van de Sande et al., 2020). The Tau value, frequently used to measure tissue or cell-type-specific gene expression (Li et al., 2022; Zhu et al., 2022), was calculated using the following formula (Kryuchkova-Mostacci & Robinson-Rechavi, 2017):

$$Tau = \frac{\sum_{i=1}^{n}(1-\hat{x}_i)}{n-1};\hat{x}_i = \frac{x_i}{\underset{1\le i\le n}{max}(x_i)} \quad (1)$$

where x_i represents the average expression value of a gene across all cells in the ith cell type out of the n cell types. Cell-type-specific TFs were identified based on a tau value of >0.85.

Gene regulatory network inference

The gene regulatory network was inferred using pySCENIC (Python-based version of SCENIC, v.0.11.2). The list of TFs was retrieved from the SCENIC GitHub repository (Van de Sande et al., 2020). Gene regulatory network inference using pySCENIC consisted of three steps. First, co-expression analysis between a predefined list of TFs and putative target genes was carried out to construct candidate regulatory modules. Next, motif enrichment analysis was performed to refine co-expression modules using human TF motif information. Finally, the activities of the discovered regulons in each individual cell were measured. To further reveal cell-type-specific regulons, differential expression analysis was performed on the activity matrix of regulons using the *FindAllMarkers* function in the Seurat package. Only those with Benjamini-Hochberg adjusted P <0.01 and avg_log_2fold-change (FC)>0.12 were defined as cell-type-specific regulons.

Gene Ontology (GO) enrichment analysis

The clusterProfiler package (v.3.18.1) in R and ClueGO plugin (v.2.5.7) in Cytoscape were used to perform GO enrichment analysis. Significantly enriched terms were determined based on a Benjamini-Hochberg corrected P-value cutoff of <0.05.

Inference of differentiation trajectory

Trajectory inference was performed using PAGA (v.1.2) with a k-nearest neighbor graph of 10 neighbors based on the top 40 principal components. The connectivity threshold between cell types was set to 0.08 to filter spurious connections.

Transcriptomic comparative analysis before and after weaning

Differential expression analysis was performed in each cell type before and after weaning. Differentially expressed genes (DEGs) were calculated using the *FindMarkers* function in Seurat and defined by Benjamini-Hochberg adjusted P<0.05 and |avg_log_2FC|>0.25.

Cell-cell communication analysis

Cell-cell communication analysis was performed using CellChat (v.1.1.3) to infer the interactions between different cell types. Ligand-receptor pairs were obtained from the receptor-ligands library of humans. Normalized counts were used as input data to CellChat and followed an analysis workflow with default parameters.

Cross-species analysis

Cross-species comparative analysis was performed to explore conservation between human and pig ceca. First, single-cell transcriptome data of the human cecum were downloaded from the Gut Cell Atlas (https://www.gutcellatlas.org/), with single-cell data of postnatal and healthy people extracted for downstream analysis. A total of 45 572 cells from the pig cecum and 20 693 cells from the human cecum were integrated using various functions in the Seurat package based on homologous genes in the two species. The top 2 000 highly variable genes in the two species were identified using the *FindVariableFeatures* function. Their intersection was used to find anchors using the *FindIntegrationAnchors* function. The two datasets were then integrated using the *IntegrateData* function. To further reveal conserved genes between the pig and human ceca, signature genes were calculated for each cell type in pigs and humans separately

using the *FindAllMarker* function in Seurat with default parameters. In both species, signature genes were defined with Benjamini-Hochberg adjusted P <0.05 and avg_log$_2$FC>0.25. Finally, the signature genes of the two species were intersected to obtain cell type-conserved genes.

RESULTS

Integrated single-cell map of developing pig cecum

We profiled single-cell transcriptomes of the pig cecum from seven individuals at four different developmental stages (Figure 1A; Supplementary Figure S1A). After quality control, we obtained 45 572 cells, which were integrated using Harmony (Korsunsky et al., 2019) and clustered into 12 major cell types (Figure 1B, C), including epithelial cells (*EPCAM*, *CDH11*, and *KRT8*), B cells (*CD19*, *CD79A*, and *CD79B*), plasma cells (*JCHAIN*, *XBP1*, and *MZB1*), myeloid cells (*CD163*, *C1QC*, and *CST3*), mast cells (*RAB27B*, *GATA2*, and *HPGDS*), T cells (*CD4*, *CD3D*, and *CD3E*), NKT cells (*CD3D*, *CD3E*, *NKG7*, and *PRF1*), enteric glial cells (*SOX10*, *PLP1*, and *HAND2*), IBP6$^-$ fibroblasts (*COL1A1*, *COL1A2*, and *DCN*), IBP6$^+$ fibroblasts (*COL1A1*, *COL1A2*, *DCN*, and *IBP6*), lymphatic endothelial cells (*PECAM1* and *LYVE1*), and vascular endothelial cells (*PECAM1* and *PLVAP*), comparable to the cell types reported in humans and mice (Elmentaite et al., 2021; Han et al., 2018, 2020; James et al., 2020; Smillie et al., 2019). Most cell types were robustly identified in all samples (Supplementary Figure S1B, C), indicating minimal impact of samples on cell-type discovery. Nevertheless, we observed substantial heterogeneity in cell composition in the cecum at different developmental stages, including an expansion of immune cells from pre-weaning (D30) to post-weaning (D42) (Supplementary Figure S1C), which may be associated with the dramatic changes in diet and ambient environment between the two stages.

At a tau value threshold of >0.85, we identified 140 TFs displaying cell-type-specific expression (Figure 1C), including *BCL11A* and *PAX5* in B cells, *FOXP3* and *LEF1* in T cells, *JDP2*, *PRNP*, and *SOX10* in enteric glial cells, *CDX2*, *EHF*, and *HNF4A* in epithelial cells, and *SOX17* in VECs. Among the identified TFs, many have been implicated in corresponding cell types in other species, e.g., *HNF4A* (Boyd et al., 2009; Tunçer et al., 2020), *SOX17* (Yao et al., 2019), and *PAX5* (Cobaleda et al., 2007; Medvedovic et al., 2011) are essential for intestinal epithelial cell, VECs, and B cell differentiation, respectively. Furthermore, several TFs displayed age-dependent expression patterns (Supplementary Figure S2A). For example, all 10 B cell-specific TFs (*BACH2*, *BCL11A*, *E2F2*, *E2F8*, *MEF2B*, *MYBL1*, *MYBL2*, *PAX5*, *PAU2F3*, and *ZNF70*) showed higher expression in the adult stages (D150 and D730), reflecting greater activity of B cells at adults than during the weaning stages; the myeloid cell-specific expression of *ARG1*, a well-characterized marker of immunosuppressive myeloid cells (Rodriguez et al., 2017; Su et al., 2021), was higher at the D30 stage and showed reduced expression with development, suggesting immunity of myeloid cells at the pre-weaning stage was more suppressed.

To further explore the key driver of cell fate and regulator of cellular functions, SCENIC (Aibar et al., 2017; Van de Sande et al., 2020) was used to infer the TF regulatory networks determined by co-expression and motif enrichment analysis. In total, 305 regulons were identified, 22 of which were cell-type-specific (Supplementary Figure S1D), including FOXP3 and GFI1 in T cells, SOX6 and SOX10 in enteric glial cells, ISX and CDX2 in epithelial cells, and SOX17 in VECs. Among these, *GFI1* is reported to regulate intestinal secretory cell differentiation and allocation, e.g., *GFI1*$^{-/-}$ mice intestines show excess enteroendocrine cells, fewer goblet cells, and no Paneth cells (Shroyer et al., 2005). *ISX* is associated with the maintenance of vitamin A metabolism (Seino et al., 2008) and controls intestinal β,β-carotene absorption (Lobo et al., 2010) in mice. These results provide a basis for future studies on the mechanisms of cell differentiation and function in the pig cecum.

Epithelial cell heterogeneity in pig cecum

Epithelial cells play important roles in digestion, absorption, and microbial interactions (Ali et al., 2020; Kong et al., 2018). Here, based on sub-clustering analysis, seven cecal epithelial subtypes were obtained, including stem cells (*OLFM4* and *SMOC2*), goblet cells (*MUC2*, *SPINK4*, and *FCGBP*), immature enterocytes (*APOBEC1* and *CA1*), mature enterocytes (*APOBEC1*, *CA1*, *SLC26A3*, and *AQP8*), BEST4$^+$ epithelial cells (*CA7*, *BEST4*, and *OTOP2*), enterocyte progenitor cells (*OLFM4*, *APOBEC1*, and *CA1*), and COL3A1$^+$ epithelial cells (*EPCAM1* and *COL3A1*) (Figure 2A, B). UMAP analysis indicated that the goblet cells were separated from other cells (Figure 2A). Partition-based graph abstraction (PAGA) analysis (Wolf et al., 2019) revealed two differentiation trajectories from stem cells via enterocyte progenitor cells to mature enterocytes and BEST4$^+$ epithelial cells, respectively (Figure 2C).

Intestinal epithelial stem cells located in crypts are responsible for the continuous renewal of the intestinal epithelial cells (Yang et al., 2021). Here, stem cells were characterized by high expression of *OLFM4* (Figure 2B), consistent with previous human colonic study (van der Flier et al., 2009). The top 200 DEGs included 50 ribosomal genes (Supplementary Table S2), consistent with previous findings in human intestinal stem cells (Burclaff et al., 2022), reflecting a state of active gene translation in intestinal epithelial stem cells.

Enterocytes perform passive barrier function and participate in digestive processes (Snoeck et al., 2005). In the current study, three enterocyte subtypes were identified, i.e., enterocyte progenitor cells, immature enterocytes, and mature enterocytes (Figure 2A, B). The enterocyte progenitor cells expressed both enterocyte marker genes *APOBEC1* and *CA1* and intestinal stem cell marker gene *OLFM4*. Immature enterocytes expressed *APOBEC1* and *CA1* but lacked *AQP8* (a water channel protein). Mature enterocytes were identified based on the expression of *APOBEC1*, *CA1*, and *AQP8*. Solute carrier (*SLC*) family genes are critical for the transport of nutrients and metabolites, such as amino acids, organic solutes, and glucose (Lin et al., 2015; Wang et al., 2020). Here, the expression of *SLC26A3* (chloride ions transporter) and *SLC16A1* (organic solute transporter) gradually increased with differentiation trajectory toward mature enterocytes (Figure 2B), reflecting gradual enhancement of transporter function in the enterocytes. The mature enterocytes exhibited a uniquely restricted expression of *AQP8* (Figure 2B), consistent with observations in the human colon (Burclaff et al., 2022).

We identified BEST4$^+$ epithelial cells in the cecum at all developmental stages (Figure 2C). This subtype is also observed in human intestines but is absent in mice (Burclaff et al., 2022; Elmentaite et al., 2021; Ito et al., 2013; Parikh

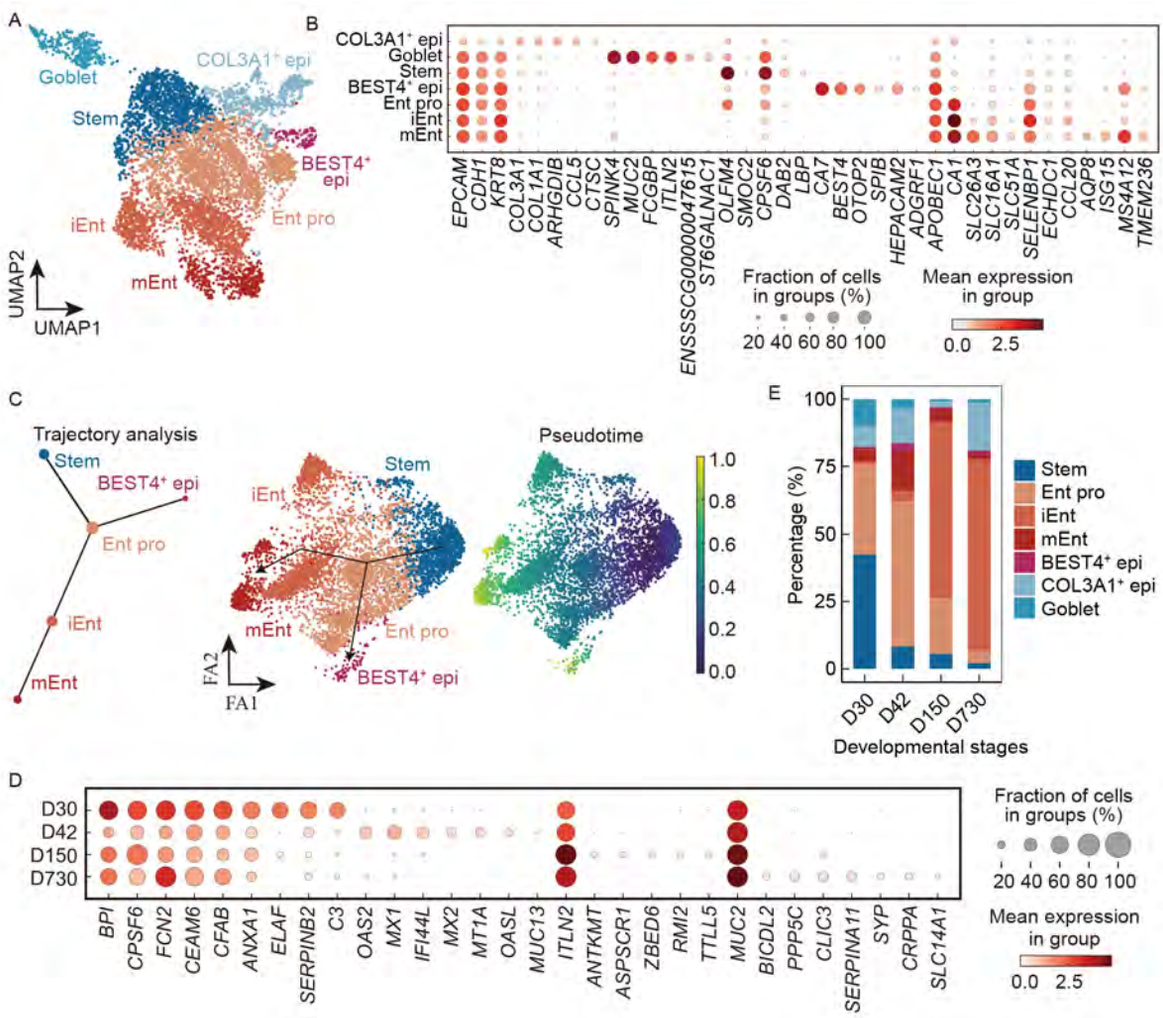

Figure 2 Heterogeneity of epithelial cells

A: UMAP of epithelial cell subtypes. Ent pro: enterocytes progenitor cells; iEnt: immature enterocytes; mEnt: mature enterocytes; epi: epithelial cells. B: Dot plot showing expression of highly expressed genes in epithelial cell subtypes. C: Trajectory analysis of enterocytes using PAGA, showing connectivity between stem cells and subpopulations of enterocytes (left), colored by cell types (middle) and pseudotime (right). D: Dot plot showing expression of highly expressed genes in goblet cells at different developmental stages. E: Relative proportions of epithelial cell subtypes at each developmental stage.

et al., 2019; Smillie et al., 2019). Notably, several marker genes, i.e., *BEST4*, *OTOP2*, and *CA7*, were conserved in both pigs and humans (Figure 2B). Based on the differentiation trajectory of BEST4$^+$ epithelial cells (Figure 2C), 67 TFs showed increased expression with differentiation from stem cells to BEST4$^+$ epithelial cells (Supplementary Table S3).

Goblet cells are responsible for producing and secreting mucin, which forms a mucus layer to support commensal bacteria (Sicard et al., 2017), protect the host epithelium from invading pathogens (Grondin et al., 2020; Specian & Oliver, 1991), and participate in the immune response (Zhang & Wu, 2020). Enrichment analysis showed that goblet cells genes were significantly enriched in GO terms "endoplasmic reticulum to Golgi vesicle-mediated transport" and "response to unfolded protein" (Supplementary Figure S3A), similar to the characteristics of goblet cells in the human gut (Burclaff et al., 2022). Based on these findings, we identified developmental stage-dependent expression of genes in goblet cells. For example, mucin-encoding *MUC2* and *ITLN2*, which participate in defense against pathogens, were expressed across all developmental stages; *C3*, an important member of complement system involved in innate immunity, showed higher expression at the D30 stage; several antiviral-related genes, such as *OAS2*, *MX1*, and *MX2*, were specifically up-regulated at the D42 stage (Figure 2D).

We observed substantial heterogeneity in the proportions of the seven epithelial cell subtypes across the four developmental stages (Figure 2E). For example, stem cells and enterocyte progenitor cells accounted for the majority of the cecal epithelium at the weaning period (D30 and D42), while enterocytes were the main cell type in the D150 and D730 stages. This reflected a physiological transition in the cecum from proliferation and development at the weaning period to food absorption and digestion at the adult stages. Notably, a marked decline in stem cells and increase in enterocyte progenitor cells and enterocytes fractions were observed from the pre-weaning (D30) to post-weaning stages (D42), which may be induced by the abrupt change in diet during the weaning period, when stem cells differentiate into enterocyte progenitor cells to prepare for absorbing nutrition from more solid and coarse feed rather than milk. Diet-induced changes in the function and fate of intestinal stem cells have

also been observed in mice (Aliluev et al., 2021).

Immune cell heterogeneity in pig cecum

Based on sub-clustering analysis, a total of 11 T lymphocyte subtypes were identified, including CD8$^+$ T (*CD8A* and *CD3E*), CD4$^+$CD8$^+$ double positive T cells (DPT) (*CD3E*, *CD8A*, and *CD4*), Tregs (*FOXP3*), γδ T (*CTSW* and *TRGC2*), RHEX$^+$ T, innate lymphoid cells (ILCs) (*KIT* and *IL23R*), cycling T (*CD3D*, *HMGB2*, *TOP2A*, and *UBE2C*), Granzyme A (high expression) natural killer T cells (GZMA^{high} NKT) (*CD3D*, *NKG7*, and *PRF1*), GZMA^{low} NKT, GZMA$^-$ NKT, and cycling NKT (*NKG7*, *HMGB2*, *TOP2A*, and *UBE2C*) (Figure 3A, B). CD8$^+$ T cells were not detected in the pre-weaning stage (D30) (Figure 3C), consistent with previous research reporting that CD8$^+$ T cells began to appear at five weeks of age in piglets (Stokes et al., 2004).

The identified RHEX$^+$ T cell subtype (Figure 3A) primarily occurred in the pre-weaning stage (D30), with its distribution decreasing over subsequent developmental stages (Figure 3C). This suggests that RHEX$^+$ T cells may play important roles in the pig cecum at the early developmental

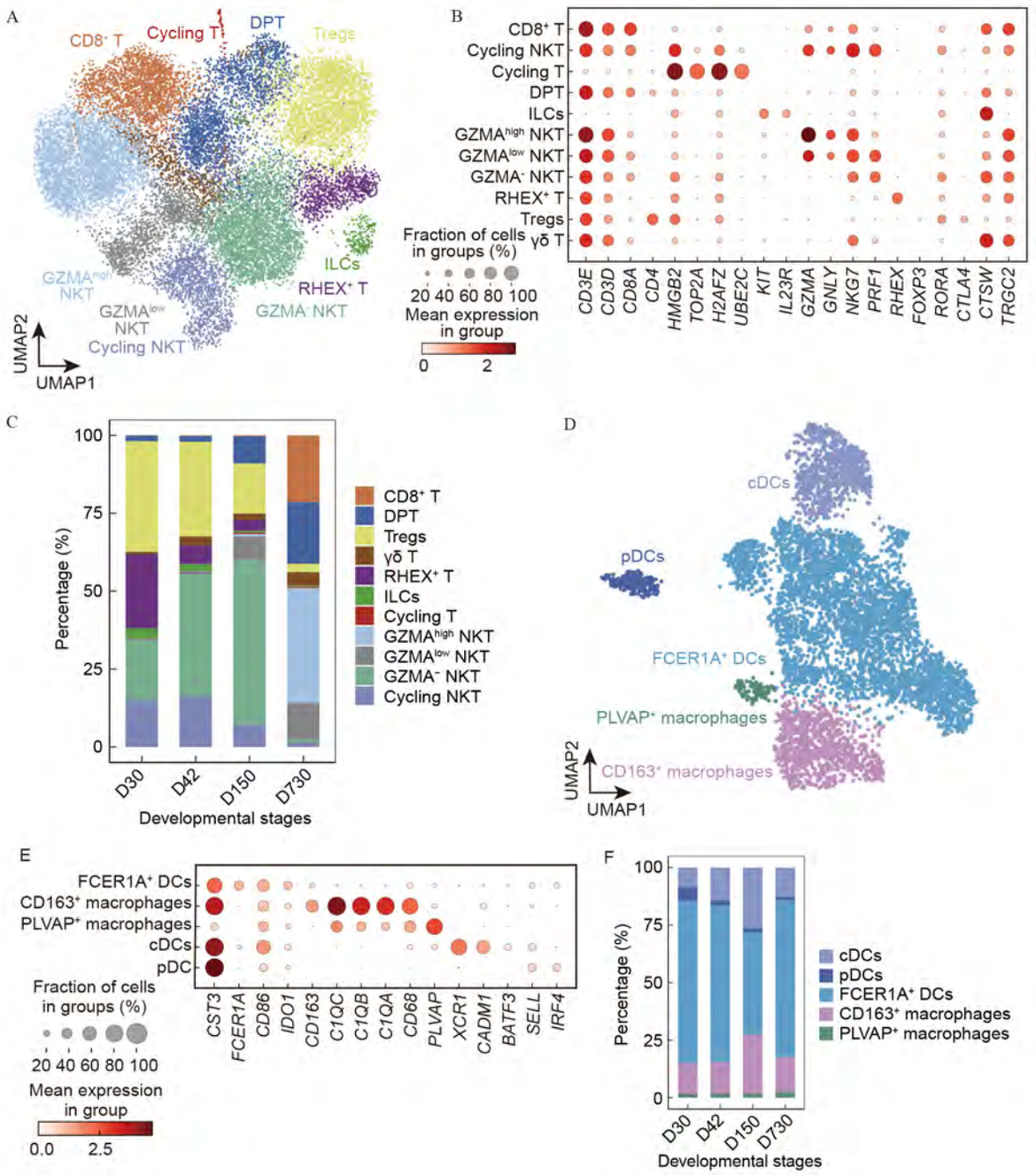

Figure 3 Heterogeneity of immune cells

A: UMAP of T cells (NKT cells plus T cells) subtypes. DPT: CD8$^+$ CD4$^+$ double positive cells; Tregs: regulatory T cells; ILCs: innate lymphocyte cells; NKT: natural killer T cells. B: Dot plot showing expression of highly expressed genes in T cells subtypes. C: Relative proportions of T cell subtypes at each developmental stage. D: UMAP of myeloid cells subtypes. cDCs: classical dendritic cells; pDCs: plasmacytoid dendritic cells. E: Dot plot showing expression of highly expressed genes in myeloid cells subtypes. F: Relative proportions of myeloid cell subtypes at each developmental stage.

stage. The relative proportion of CD8$^+$ T cells and GZMA^{low} NKT cells tended to increase, while Tregs appeared to decrease with development (Figure 3C; Supplementary Figure S3B), suggesting an increased immune response by these cells in the cecum during development. Cycling NKT cells were also enriched in the D30 and D42 stages, while DPT cells were enriched in the D150 and D730 stages (Figure 3C).

The myeloid cells were clustered into five sub-populations, including CD163$^+$ macrophages (*CD163*, *C1QC*, and *C1QB*), PLVAP$^+$ macrophages, FCER1A$^+$ DCs (*FCER1A* and *IDO1*), cDCs (*XCR1*, *CADM1*, and *BATF3*) and plasmacytoid dendritic cells (pDCs, *SELL* and *IRF4*) (Figure 3D, E; Supplementary Figure S3C). Among these, PLVAP$^+$ macrophages expressed both *C1QC* and *C1QB* genes, as well as the VECs marker *PLVAP*, but lacked the *CD163* gene (Figure 3E). The pDCs, a relatively rare cell type linking innate and adaptive immunity (McKenna et al., 2005), showed a gradient decrease from the D30 to D730 stages (Figure 3F).

Fibroblasts and endothelial cell heterogeneity in pig cecum

The fibroblasts were clustered into five sub-populations, including two IBP6$^-$ fibroblast subtypes (IBP6$^-$CCL5$^-$ fib and IBP6$^-$CCL5$^+$ fib) and three IBP6$^+$ fibroblast subtypes (IBP6$^+$IL6$^+$ fib, IBP6$^+$SEMA3C$^+$ fib, and IBP6$^+$CPXM2$^+$ fib), which all expressed fibroblast marker genes *COL1A1*, *COL1A2*, and *DCN* (Figure 4A, B). The IBP6$^-$CCL5$^+$ fib subtype was distinguished by *CCL5* expression but a lack of *IBP6* (Figure 4B), while IBP6$^-$CCL5$^+$ fib also showed *IL2RB* and *CCL4* expression (Figure 4B). Enrichment analysis revealed that the IBP6$^-$CCL5$^+$ fib subtype genes were significantly enriched in the GO term "positive regulation of developmental growth" (Supplementary Figure S4A). The IBP6$^-$CCL5$^+$ fib subtype appeared at the D42 stage and showed a gradient increase with development (Figure 4C). These findings suggested that the IBP6$^-$CCL5$^+$ fib subtype plays an important role in promoting growth and development, especially in late-stage cecal tissue. Enrichment analysis revealed that the three IBP6$^+$ fibroblasts subtypes were significantly enriched in genes involved in "positive regulation of angiogenesis", implying a key role in angiogenesis (Supplementary Figure S4A). The relative proportion of the IBP6$^+$CPXM2$^+$ fib subtype tended to increase with development (Figure 4C), while the IBP6$^+$IL6$^+$ fib subtype was mainly enriched in the D30 and D42 stages, showing a gradient decrease with development (Figure 4C).

Endothelial cells (ECs) were clustered into six sub-populations, including LYVEL$^+$ LECs (*PROX1*, *RELN*, and *LYVE1*), LYVE1$^-$ LECs (*PROX1* and *RELN*), venous ECs (*PLVAP*, *ADGRG6*, and *ACKR1*), venous capillary ECs (*PLVAP, RGCC*, and *SGK1*), capillary ECs (*EDNRB*, *RGCC*, and *CD36*), and arterial ECs (*TMEM100*, *SEMA3G*, and *GJA5*) (Figure 4A, B; Supplementary Figure S4B). Among these, LYVE1$^-$ LECs expressed LECs markers *PROX1* and *RELN* but did not express *PLVAP*. Furthermore, LYVE1$^-$ LECs also differed based on the expression of *SCG3*, *ECRG4*, *SLC41A1*, and *S100A4* (Figure 4B). Venous capillary ECs expressed both venous marker *PLVAP* and capillary markers *RGCC* and *SGK1* (Figure 4B), similar to observations

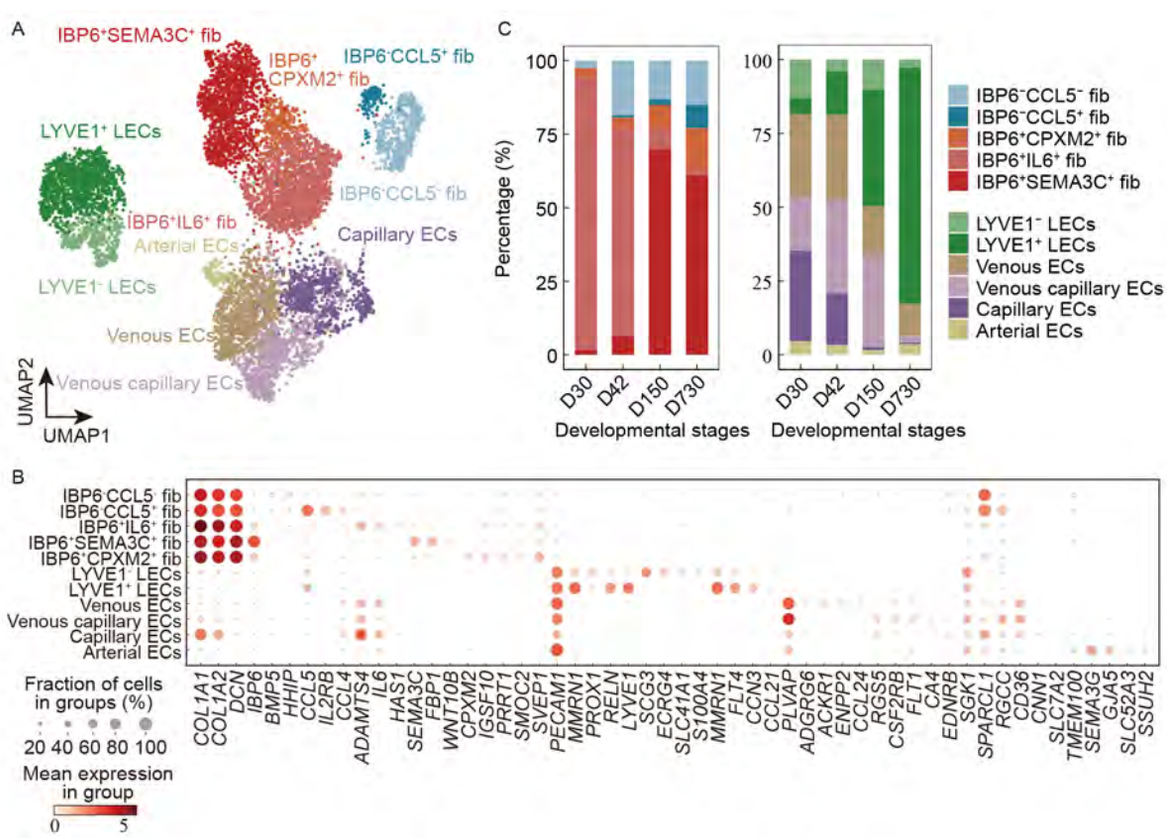

Figure 4 Heterogeneity of fibroblasts and endothelial cells

A: UMAP of fibroblasts and endothelial cell subtypes. fib: fibroblasts; LECs: lymphatic endothelial cells; ECs: endothelial cells. B: Dot plot showing expression of highly expressed genes in fibroblasts and endothelial cell subtypes. C: Relative proportions of fibroblast subtypes (left) and endothelial cell subtypes (right) at each developmental stage.

in humans and mice (Fawkner-Corbett et al., 2021; Kalucka et al., 2020). Additionally, the relative proportion of LYVE1$^+$ LECs tended to increase with developmental stages, particularly from D150 to D730 (Figure 4C).

Age-associated gene expression changes in different cell types in pig cecum

The weaning process, an important event in pig production, induces dramatic functional and morphological changes in the intestine (Campbell et al., 2013; Tang et al., 2022; Zheng et al., 2021). To explore the changes in molecular characteristics during the weaning process at the single-cell level, we identified weaning-associated gene transcriptions in different cecal cell types. In total, we identified 1 869 DEGs, which were differentially expressed in at least one cell type of the D42 cecum compared to the D30 cecum (Figure 5A; Supplementary Table S4). The most affected cell types during weaning included epithelial cells, myeloid cells, IBP6$^+$ fibroblasts, IBP6$^-$ fibroblasts, and NKT cells, with 648, 300, 180, 174, and 151 DEGs in the D42 compared to the D30 cecal cell types, respectively (Figure 5A). Mitochondrial genes were up-regulated in multiple cell types in the post-weaning cecum compared to the pre-weaning cecum (Figure 5B). *COX2*, the inducible form of cyclo-oxygenase, which catalyzes arachidonic acid to produce prostaglandins (Choi et al., 2009), was significantly up-regulated in the NKT, T, myeloid, and epithelial cells. *ND2*, which encodes mitochondrially NADH: ubiquinone oxidoreductase core subunit 2, was significantly up-regulated in NKT, T, VECs, and epithelial cells. Enrichment analysis of DEGs revealed the activation of immune-related pathways in several immune cells, including T, NKT, and B cells (Figure 5C). In addition, genes involved in the transportation of nutrients were down-regulated in epithelial cells (Figure 5C). These results imply that dramatic changes occur in gut gene transcription due to weaning stress.

Receptor-ligand analysis revealed heterogeneity in cell-cell interactions across developmental stages

Tissues achieve functionality through interactions among different cell types. Based on cellular communication analysis using CellChat (Jin et al., 2021), we explored potential cell-type interactions and heterogeneities across different developmental stages. On average, 100 interactions at each developmental stage were detected based on a *P*-value threshold significance of 0.05 (Figure 6A; Supplementary Table S5). Total cellular interaction strength gradually increased with development (Figure 6A).

We next compared outgoing and incoming interaction strengths to identify cell types showing significant changes in signaling activities across different developmental stages. Results revealed that IBP6$^+$ fibroblasts were the main signal senders at the D30 stage, while IBP6$^-$ fibroblasts assumed this role at other stages (Figure 6B). IBP6$^+$ but not IBP6$^-$ fibroblasts used the vascular endothelial growth factor (*VEGFD* and *VEGFC*) signaling pathway for endothelial cell communication (Figure 6C, Supplementary Figure S5A). Given the pivotal role of VEGFs and their endothelial tyrosine kinase receptors in angiogenesis and lymph-angiogenesis (Lohela et al., 2009), this suggests an important regulatory function of IBP6$^+$ fibroblasts in angiogenesis.

Extensive interactions between immune and non-immune cells were also identified. The incoming interaction strength for T cells gradually increased with development (Figure 6B), suggesting increasing involvement of different cell types in mediating the T cell immune response. Additionally, *GZMA* was identified as an outgoing signal from NKT cells, predicted to interact with *F2RL1/F2RL2* in epithelial cells and IBP6$^+$ fibroblasts at the D730 stage (Figure 6D; Supplementary Figure S5A, B). The *GZMA*- encoded serine protease promotes aberrant cell death in tumorigenic and virus-infected cells (Catalan et al., 2012; Chowdhury & Lieberman, 2008; Topham & Hewitt, 2009), suggesting a potential host strategy to lyse infected cells, and thereby provide protection and promote cell turnover. Furthermore, *CCL5-ACKR1* interactions between NKT cells and VECs were also observed at D730 (Figure 6D; Supplementary Figure S5A, B). *CCL5* plays an important role in immune responses and inflammation (Marques et al., 2013), while *ACKR1* is thought to clear inflammatory CC and CXC chemokines to regulate acute inflammatory responses (Davis et al., 2015; Wan et al., 2015). Overall, these results reveal the important role of immune and non-immune cell interactions in intestinal homeostasis.

Conservativeness of cell-type gene expression in pig and human ceca

To better understand the conservation of genes between human and pig intestines, we compared our data with published transcriptome data of the human cecum (Elmentaite et al., 2021). In total, 45 572 cells from the pig cecum and 20 693 cells from the human cecum were integrated for cross-species comparison (Haghverdi et al., 2018). Unsupervised graph-based clustering showed that the same cell types in humans and pigs were grouped together (Figure 7A). We next examined gene expression conservation between the pig and human ceca. Results showed that marker genes defining cell types were conserved in both pigs and humans (Figure 7B), including *MUC2* and *FCGBP* in goblet cells, *PECAM1* and *PLVAP* in endothelial cells, *SLC26A3* and *AQP8* in enterocytes, and *CD19* and *CD79A* in B cells. *MUC2* is secreted by goblet cells to form an insoluble mucous barrier to protect the gut lumen (Grondin et al., 2020), while *AQP8* plays an important role in water absorption (Wang et al., 2020). In addition, results also revealed several conserved TFs in both the pig and human single-cell datasets (Figure 7C), including *SOX18* in endothelial cells, *CREB3L1* and *SPDEF* in goblet cells, *CDX2* in enterocytes, and *PAX5* in B cells. Of note, *SOX18* is essential for endothelial cell differentiation (Yao et al., 2019), while *SPDEF* is required for goblet cell mucus production and differentiation (Song et al., 2017). In summary, these observations confirmed the conservation of gene expression and functions in the pig and human ceca.

DISCUSSION

The intestinal tract, vital for digestion, absorption, and immunological functions, has been extensively characterized through single-cell transcriptomics in humans and mice (Burclaff et al., 2022; Elmentaite et al., 2021; Haber et al., 2017). However, in pigs, investigations into cellular compositions and gene expression profiles in the intestinal tract at different developmental stages remain unexplored. In the present study, we conducted a single-cell transcriptomic analysis of the pig cecum at ages 30, 42, 150 and 730 days, and further explored cellular heterogeneity across different developmental stages, particularly before and after weaning, which is characterized by marked shifts in diet and environmental conditions (Blavi et al., 2021). Our results indicated an expansion in immune cells from the pre-weaning

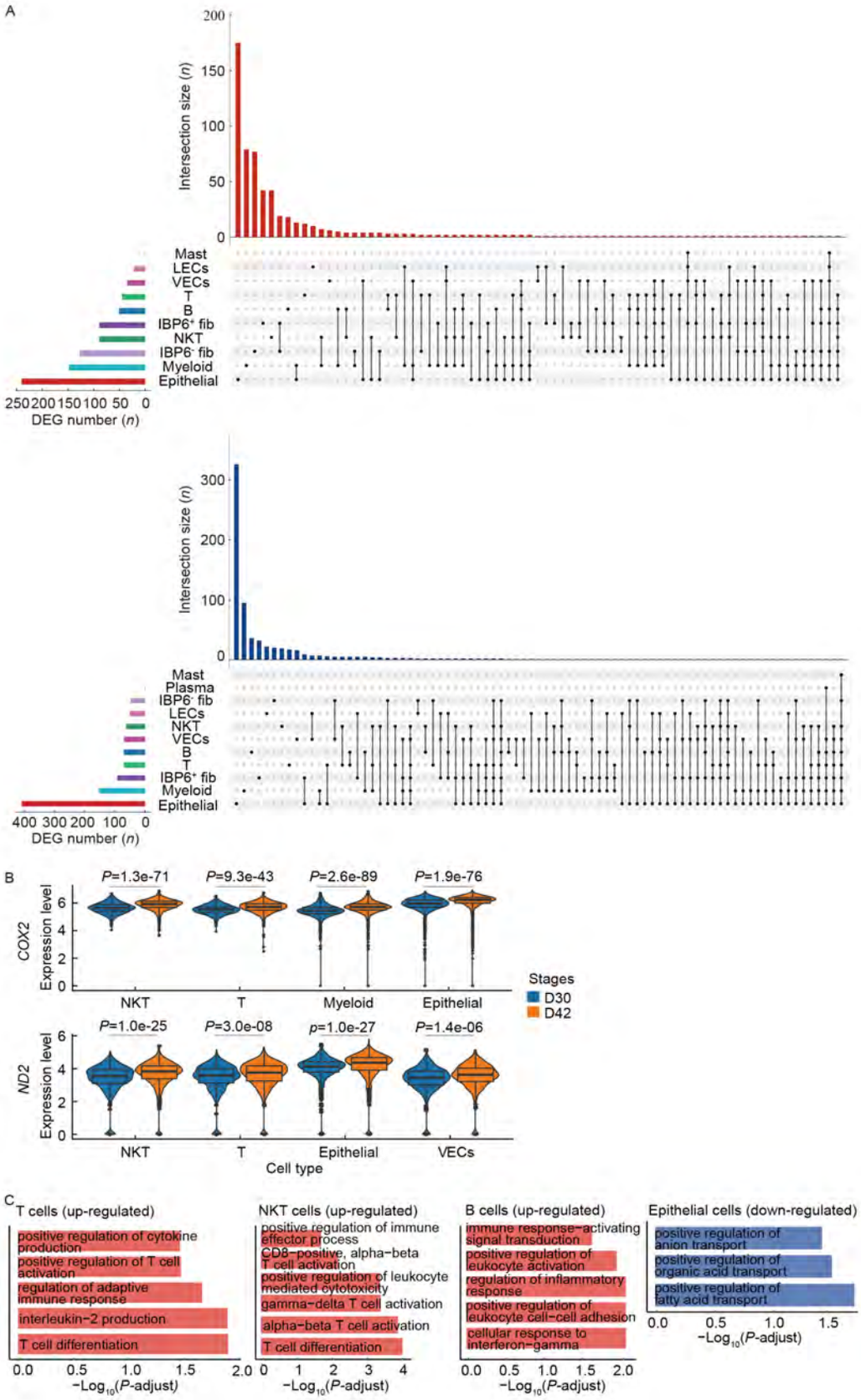

Figure 5 Weaning-associated changes in gene expression levels in different cell types

A: Intersection plot showing number of DEGs (top: up-regulated genes; bottom: down-regulated genes) in different cell types. Left horizontal bar plot shows total number of DEGs in each cell type. Top bar plot shows number of DEGs for each intersection. Abbreviations of cell types are the same as in Figure 1. B: Violin plot combined with box plot showing transcription levels of *COX2* and *ND2* in D30 and D42 stages, respectively. *P*-value refers to Benjamini-Hochberg adjusted *P*-value. C: GO pathways significantly enriched in up-regulated or down-regulated genes in T, NKT, B, and epithelial cells at D42 stage compared to D30 stage.

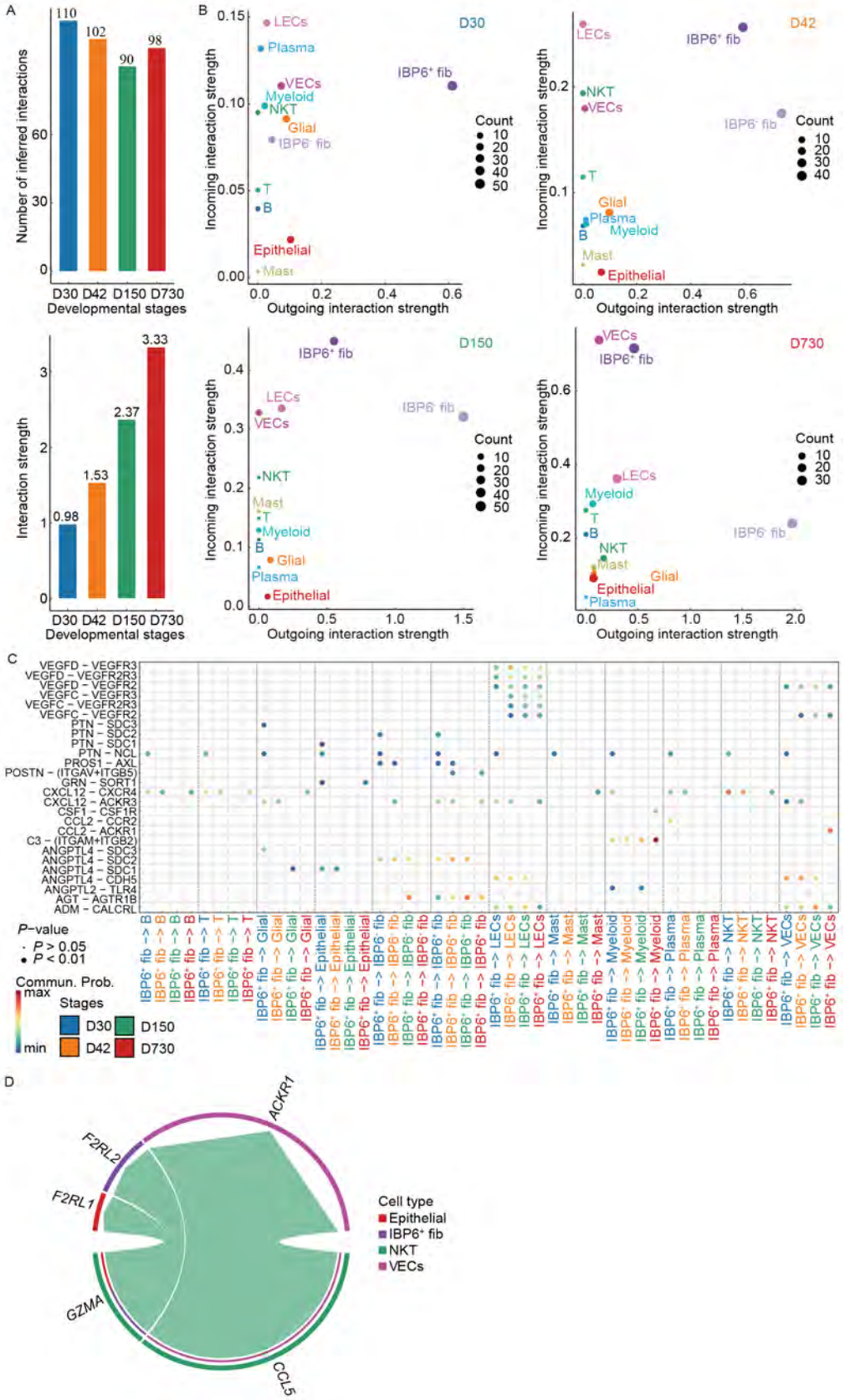

Figure 6 Cell-cell communication in developing pig cecum

A: Total number and strength of inferred cell-cell interactions at each developmental stage. B: Scatter plot showing strength of signals sent and received by each cell type at each developmental stage. Abbreviations of cell types are the same as in Figure 1. C: Bubble plot showing significant receptor-ligand pairs of IBP6$^+$ fibroblasts for communication with other cell types at different developmental stages. D: Chord diagram showing all interactions sent from NKT cells at D730 stage.

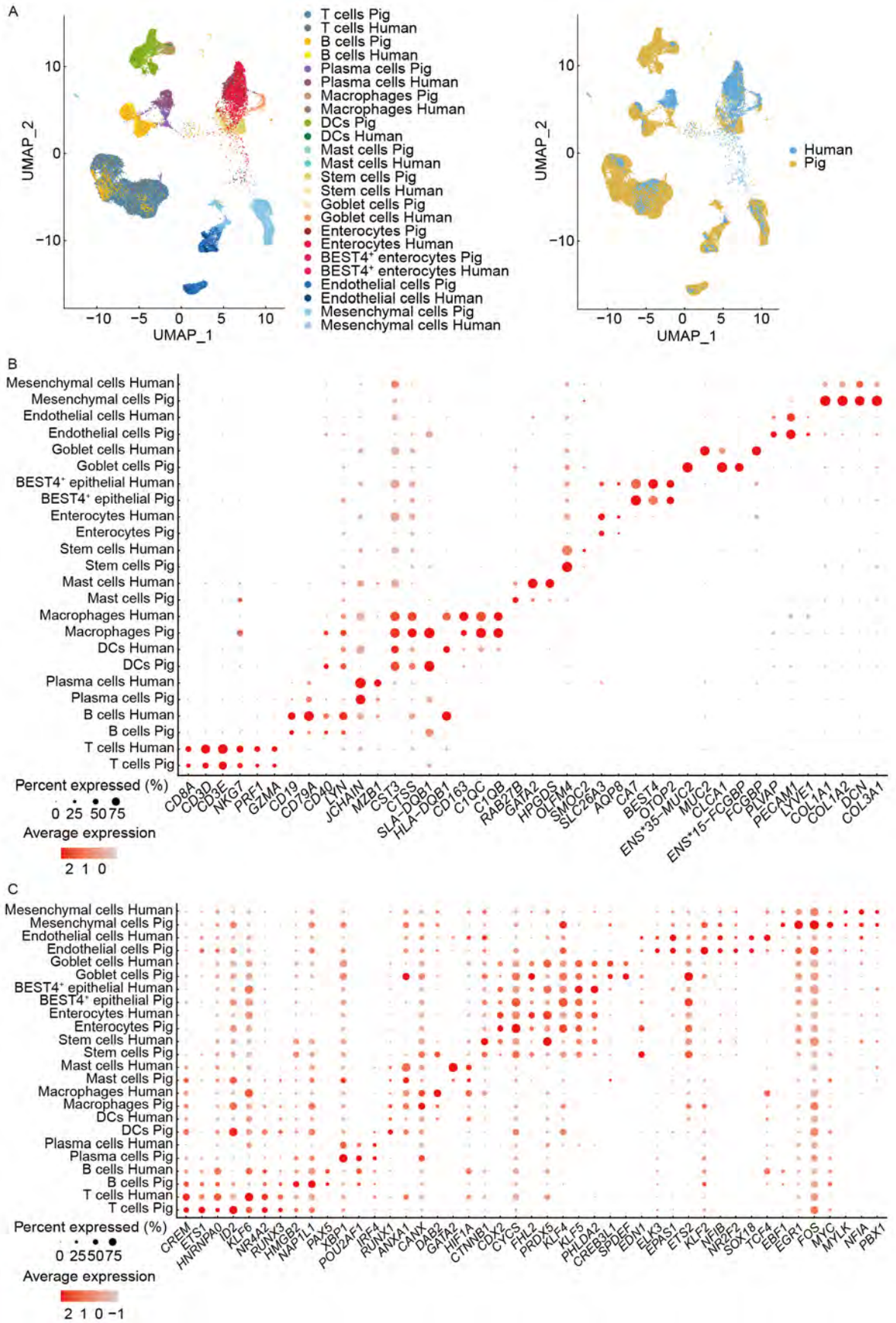

Figure 7 Comparison of human and pig cecum single-cell data

A: UMAP plot showing integration of human and pig cecum single-cell data, colored by cell type (left) and species (right). DCs: dendritic cells. B: Dot plot showing expression of marker genes between human and pig cecum single-cell data. ENS*35-MUC2: ENSSSCG00000040035-MUC2, ENS*15-FCGBP: ENSSSCG00000027515-FCGBP. C: Dot plot showing expression of TFs between human and pig cecum single-cell data.

(D30) to post-weaning stages (D42), as well as a decline in epithelial stem cells along developmental stages, particularly from D30 to D42. We identified 848 up-regulated and 1 021 down-regulated genes after weaning. Among these genes, certain mitochondrial genes were up-regulated in different cell types in the D42-stage cecum, including *COX2* in T, NKT, epithelial, and myeloid cells and *COX1* in epithelial cells. *COX1* and *COX2* are key enzymes involved in the catalysis of arachidonic acid to produce prostaglandins (Choi et al., 2009), which are implicated in inflammatory processes (Ricciotti & Fitzgerald, 2011). Concurrently, we noted that up-regulated genes were predominantly enriched in immune-activation related pathways, including "CD8-positive, alpha-beta T cell activation" and "positive regulation of immune effector process" in NKT cells, and "immune response-activation signal transduction" and "positive regulation of leukocyte activation" in B cells. These findings provide insight into physiological changes that occur during weaning and lay the groundwork for understanding the underlying mechanisms of weaning stress in the pig cecum.

We identified two major fibroblast subtypes, which were distinguished by *IBP6* expression and displayed distinct cell-cell crosstalk patterns across the different developmental stages. Notably, IBP6$^+$ fibroblasts acted as the dominant signal senders at the D30 stage, while IBP6$^-$ fibroblasts assumed this role at the other stages. Results indicated that IBP6$^+$ fibroblasts used *PTN/NCL* to communicate with all other cell types, but only at the D30 stage. *PTN*, a secreted growth factor, is associated with cell differentiation, growth, and proliferation (González-Castillo et al., 2015). IBP6$^+$ but not IBP6$^-$ fibroblasts used *C3-(ITGAM_ITGB2)* to communicate with myeloid cells at the D30 and D42 stages. *C3*, also known as complement C3, plays a critical role in the innate immune response (Bohlson et al., 2014). Additionally, IBP6$^+$ but not IBP6$^-$ fibroblasts communicated with endothelial cells (LECs and VECs) through *VEGFD/VEGFC-VEGFR3/VEGFR2* pairs. VEGFs and their endothelial tyrosine kinase receptors play key roles in angiogenesis (Lohela et al., 2009). These observations suggest important roles of IBP6$^+$ fibroblasts in the regulation of innate immunity and angiogenesis, as well as the promotion of cell growth and differentiation, especially in early-stage cecal tissue.

Gut immune cells account for 70%–80% of all immune cells in the body (Agace & McCoy, 2017; Mowat & Agace, 2014; Wiertsema et al., 2021). These immune cells are essential for normal physiology and pathogen defense (James et al., 2022). Our data revealed extensive interactions between immune and non-immune cells at the different developmental stages, including interactions between NKT and epithelial cells, plasma and enteric glial cells, and myeloid cells and LECs. At the D730 stage, NKT cells sent GZMA signals to interact with epithelial cells and IBP6$^+$ fibroblasts. *GZMA* encodes serine protease, which induces aberrant cell death of tumorigenic and virus-infected cells (Catalan et al., 2012; Chowdhury & Lieberman, 2008; Topham & Hewitt, 2009). Plasma cells used *MIF-ACKR3* to communicate with non-immune cells at the D30 and D42 stages, including enteric glial cells, VECs, LECs, and IBP6$^+$ fibroblasts. The *MIF* ligand is an immunoregulatory cytokine and displays direct chemokine-like functions (Grieb et al., 2010), while receptor *ACKR3* is considered a scavenger receptor gene (Duval et al., 2022). Based on these results, we hypothesize that intestinal immune and non-immune cells may communicate with each other using ligand and receptor pairs to maintain intestinal homeostasis. However, the interactions between these receptor ligands and cells need to be further verified with spatial transcriptomic analysis.

This study has several limitations worth mentioning. Due to the limited number of cells, not all epithelial subtypes were captured, including tuft and enteroendocrine cells, possibly due to insufficient or prolonged tissue digestion. Consequently, observations regarding cell-type proportions and their temporal shifts during development, particularly the hypothesis suggesting diet-induced changes in stem cell composition from the pre-weaning to post-weaning stages, require further experimental verification based on other approaches, such as immunofluorescence quantification and flow sorting. Future research should expand single-cell datasets and incorporate multi-omics analyses to elucidate the cellular characteristics of the pig cecum more comprehensively.

DATA AVAILABILITY

Datasets generated in this study were deposited in the Genome Sequence Archive (GSA) database (https://ngdc.cncb.ac.cn/gsa/) under accession number CRA010843, Science Data Bank (doi:10.57760/sciencedb.j00139.00082) and NCBI under BioProjectID PRJNA1036035.

SUPPLEMENTARY DATA

Supplementary data to this article can be found online.

COMPETING INTERESTS

The authors declare that they have no competing interests.

AUTHORS' CONTRIBUTIONS

Experimental design and conception: L.S.H.; investigation: Y.Y.X., B.Y., Q.Z., F.H., L.R., T.X.Y., S.Y.Y., L.P.C., L.X., X.X.Z., and J.W.Y.; formal analysis: Y.Y.X.; writing-original draft: Y.Y.X.; writing-review & editing: L.S.H. and B.Y.; experimental organization and analysis supervision: L.S.H. All authors read and approved the final version of the manuscript.

ACKNOWLEDGEMENTS

We would like to thank colleagues in the National Key Laboratory for Swine Genetic Improvement and Germplasm Innovation, Jiangxi Agricultural University for their help in collecting samples and providing suggestions during analysis.

REFERENCES

Agace WW, McCoy KD. 2017. Regionalized development and maintenance of the intestinal adaptive immune landscape. *Immunity*, **46**(4): 532−548.

Aibar S, González-Blas CB, Moerman T, et al. 2017. SCENIC: single-cell regulatory network inference and clustering. *Nature Methods*, **14**(11): 1083−1086.

Ali A, Tan HY, Kaiko GE. 2020. Role of the intestinal epithelium and its interaction with the microbiota in food allergy. *Frontiers in Immunology*, **11**: 604054.

Aliluev A, Tritschler S, Sterr M, et al. 2021. Diet-induced alteration of intestinal stem cell function underlies obesity and prediabetes in mice. *Nature Metabolism*, **3**(9): 1202−1216.

Blavi L, Solà-Oriol D, Llonch P, et al. 2021. Management and feeding strategies in early life to increase piglet performance and welfare around weaning: a review. *Animals*, **11**(2): 302.

Bohlson SS, O'Conner SD, Hulsebus HJ, et al. 2014. Complement, C1q, and C1q-related molecules regulate macrophage polarization. *Frontiers in Immunology*, **5**: 402.

Boyd M, Bressendorff S, Møller J, et al. 2009. Mapping of HNF4α target genes in intestinal epithelial cells. *BMC Gastroenterology*, **9**: 68.

Brown K, Abbott DW, Uwiera RRE, et al. 2018. Removal of the cecum affects intestinal fermentation, enteric bacterial community structure, and acute colitis in mice. *Gut Microbes*, **9**(3): 218−235.

Burclaff J, Bliton RJ, Breau KA, et al. 2022. A proximal-to-distal survey of healthy adult human small intestine and colon epithelium by single-cell transcriptomics. *Cellular and Molecular Gastroenterology and Hepatology*, **13**(5): 1554−1589.

Campbell JM, Crenshaw JD, Polo J. 2013. The biological stress of early weaned piglets. *Journal of Animal Science and Biotechnology*, **4**(1): 19.

Catalan E, Sanchez-Martinez D, Pardo J. 2012. GZMA (granzyme A (granzyme 1, cytotoxic T-lymphocyte-associated serine esterase 3)). *Atlas of Genetics and Cytogenetics in Oncology and Haematology*, **16**(2): 123−126.

Chassaing B, Kumar M, Baker MT, et al. 2014. Mammalian gut immunity. *Biomedical Journal*, **37**(5): 246−258.

Chen SF, Zhou YQ, Chen YR, et al. 2018. fastp: an ultra-fast all-in-one FASTQ preprocessor. *Bioinformatics*, **34**(17): i884−i890.

Choi SH, Aid S, Bosetti F. 2009. The distinct roles of cyclooxygenase-1 and -2 in neuroinflammation: implications for translational research. *Trends in Pharmacological Sciences*, **30**(4): 174−181.

Chowdhury D, Lieberman J. 2008. Death by a thousand cuts: granzyme pathways of programmed cell death. *Annual Review of Immunology*, **26**: 389−420.

Cobaleda C, Schebesta A, Delogu A, et al. 2007. Pax5: the guardian of B cell identity and function. *Nature Immunology*, **8**(5): 463−470.

Dabareiner RM, White II NA. 1997. Diseases and surgery of the cecum. *Veterinary Clinics of North America:Equine Practice*, **13**(2): 303−315.

Davis MB, Walens A, Hire R, et al. 2015. Distinct transcript isoforms of the atypical chemokine receptor 1 (ACKR1)/duffy antigen receptor for chemokines (DARC) gene are expressed in lymphoblasts and altered isoform levels are associated with genetic ancestry and the duffy-null allele. *PLoS One*, **10**(10): e0140098.

Duval V, Alayrac P, Silvestre JS, et al. 2022. Emerging roles of the atypical chemokine receptor 3 (ACKR3) in cardiovascular diseases. *Frontiers in Endocrinology*, **13**: 906586.

Elmentaite R, Kumasaka N, Roberts K, et al. 2021. Cells of the human intestinal tract mapped across space and time. *Nature*, **597**(7875): 250−255.

Fawkner-Corbett D, Antanaviciute A, Parikh K, et al. 2021. Spatiotemporal analysis of human intestinal development at single-cell resolution. *Cell*, **184**(3): 810−826.e23.

Gerrits RJ, Lunney JK, Johnson LA, et al. 2005. Perspectives for artificial insemination and genomics to improve global swine populations. *Theriogenology*, **63**(2): 283−299.

González-Castillo C, Ortuño-Sahagún D, Guzmán-Brambila C, et al. 2015. Pleiotrophin as a central nervous system neuromodulator, evidences from the hippocampus. *Frontiers in Cellular Neuroscience*, **8**: 443.

Grieb G, Merk M, Bernhagen J, et al. 2010. Macrophage migration inhibitory factor (MIF): a promising biomarker. *Drug News & Perspectives*, **23**(4): 257−64.

Grondin JA, Kwon YH, Far PM, et al. 2020. Mucins in intestinal mucosal defense and inflammation: learning from clinical and experimental studies. *Frontiers in Immunology*, **11**: 2054.

Haber AL, Biton M, Rogel N, et al. 2017. A single-cell survey of the small intestinal epithelium. *Nature*, **551**(7680): 333−339.

Haghverdi L, Lun ATL, Morgan MD, et al. 2018. Batch effects in single-cell RNA-sequencing data are corrected by matching mutual nearest neighbors. *Nature Biotechnology*, **36**(5): 421−427.

Han L, Wei XY, Liu CY, et al. 2022. Cell transcriptomic atlas of the non-human primate *Macaca fascicularis*. *Nature*, **604**(7907): 723–731.

Han XP, Wang RY, Zhou YC, et al. 2018. Mapping the mouse cell atlas by microwell-seq. *Cell*, **172**(5): 1091−1107.e17.

Han XP, Zhou ZM, Fei LJ, et al. 2020. Construction of a human cell landscape at single-cell level. *Nature*, **581**(7808): 303−309.

Ito G, Okamoto R, Murano T, et al. 2013. Lineage-specific expression of bestrophin-2 and bestrophin-4 in human intestinal epithelial cells. *PLoS One*, **8**(11): e79693.

James KR, Elmentaite R, Teichmann SA, et al. 2022. Redefining intestinal immunity with single-cell transcriptomics. *Mucosal Immunology*, **15**(4): 531−541.

James KR, Gomes T, Elmentaite R, et al. 2020. Distinct microbial and immune niches of the human colon. *Nature Immunology*, **21**(3): 343−353.

James SP. 1993. The gastrointestinal mucosal immune system. *Digestive Diseases*, **11**(3): 146−156.

Jin SQ, Guerrero-Juarez CF, Zhang LH, et al. 2021. Inference and analysis of cell-cell communication using CellChat. *Nature Communications*, **12**(1): 1088.

Kalucka J, de Rooij LPMH, Goveia J, et al. 2020. Single-cell transcriptome atlas of murine endothelial cells. *Cell*, **180**(4): 764−779.e20.

Kong SS, Zhang YH, Zhang WQ. 2018. Regulation of intestinal epithelial cells properties and functions by amino acids. *BioMed Research International*, **2018**: 2819154.

Korsunsky I, Millard N, Fan J, et al. 2019. Fast, sensitive and accurate integration of single-cell data with Harmony. *Nature Methods*, **16**(12): 1289−1296.

Kryuchkova-Mostacci N, Robinson-Rechavi M. 2017. A benchmark of gene expression tissue-specificity metrics. *Briefings in Bioinformatics*, **18**(2): 205−214.

Li HJ, Janssens J, De Waegeneer M, et al. 2022. Fly cell atlas: a single-nucleus transcriptomic atlas of the adult fruit fly. *Science*, **375**(6584): eabk2432.

Liao DH, Zhao JB, Gregersen H. 2009. Gastrointestinal tract modelling in health and disease. *World Journal of Gastroenterology*, **15**(2): 169−176.

Lin L, Yee SW, Kim RB, et al. 2015. SLC transporters as therapeutic targets: emerging opportunities. *Nature Reviews Drug Discovery*, **14**(8): 543−560.

Lobo GP, Hessel S, Eichinger A, et al. 2010. ISX is a retinoic acid-sensitive gatekeeper that controls intestinal β, β-carotene absorption and vitamin A production. *The FASEB Journal*, **24**(6): 1656−1666.

Lohela M, Bry M, Tammela T, et al. 2009. VEGFs and receptors involved in angiogenesis versus lymphangiogenesis. *Current Opinion in Cell Biology*, **21**(2): 154−165.

Lunney JK, Van Goor A, Walker KE, et al. 2021. Importance of the pig as a human biomedical model. *Science Translational Medicine*, **13**(621): eabd5758.

Marques RE, Guabiraba R, Russo RC, et al. 2013. Targeting CCL5 in inflammation. *Expert Opinion on Therapeutic Targets*, **17**(12): 1439−1460.

McKenna K, Beignon AS, Bhardwaj N. 2005. Plasmacytoid dendritic cells: linking innate and adaptive immunity. *Journal of Virology*, **79**(1): 17−27.

Medvedovic J, Ebert A, Tagoh H, et al. 2011. Pax5: a master regulator of B cell development and leukemogenesis. *Advances in Immunology*, **111**: 179−206.

Mowat AM, Agace WW. 2014. Regional specialization within the intestinal immune system. *Nature Reviews Immunology*, **14**(10): 667−685.

Parikh K, Antanaviciute A, Fawkner-Corbett D, et al. 2019. Colonic epithelial cell diversity in health and inflammatory bowel disease. *Nature*, **567**(7746): 49−55.

Ricciotti E, Fitzgerald GA. 2011. Prostaglandins and inflammation. *Arteriosclerosis, Thrombosis, and Vascular Biology*, **31**(5): 986−1000.

Rodriguez PC, Ochoa AC, Al-Khami AA. 2017. Arginine metabolism in myeloid cells shapes innate and adaptive immunity. *Frontiers in Immunology*, **8**: 93.

Seino Y, Miki T, Kiyonari H, et al. 2008. Isx participates in the maintenance of vitamin A metabolism by regulation of β-carotene 15, 15'-monooxygenase (Bcmo1) expression. *Journal of Biological Chemistry*, **283**(8): 4905−4911.

Shroyer NF, Wallis D, Venken KJT, et al. 2005. *Gfi1* functions downstream of *Math1* to control intestinal secretory cell subtype allocation and differentiation. *Genes & Development*, **19**(20): 2412−2417.

Sicard JF, Le Bihan G, Vogeleer P, et al. 2017. Interactions of intestinal bacteria with components of the intestinal mucus. *Frontiers in Cellular and Infection Microbiology*, **7**: 387.

Smillie CS, Biton M, Ordovas-Montanes J, et al. 2019. Intra- and inter-cellular rewiring of the human colon during ulcerative colitis. *Cell*, **178**(3): 714−730.e22.

Snoeck V, Goddeeris B, Cox E. 2005. The role of enterocytes in the intestinal barrier function and antigen uptake. *Microbes and Infection*, **7**(7-8): 997−1004.

Song J, Heijink IH, Kistemaker LEM, et al. 2017. Aberrant DNA methylation and expression of SPDEF and FOXA2 in airway epithelium of patients with COPD. *Clinical Epigenetics*, **9**: 42.

Specian RD, Oliver MG. 1991. Functional biology of intestinal goblet cells. *American Journal of Physiology-Cell Physiology*, **260**(2 Pt 1): C183–C193.

Stokes CR, Bailey M, Haverson K, et al. 2004. Postnatal development of intestinal immune system in piglets: implications for the process of weaning. *Animal Research*, **53**(4): 325−334.

Stumpff F, Manneck D, Martens H. 2019. Unravelling the secrets of the caecum. *Pflügers Archiv - European Journal of Physiology*, **471**(7): 925−926.

Su XM, Xu YL, Fox GC, et al. 2021. Breast cancer-derived GM-CSF regulates arginase 1 in myeloid cells to promote an immunosuppressive microenvironment. *Journal of Clinical Investigation*, **131**(20): e145296.

Tang XP, Xiong KN, Fang RJ, et al. 2022. Weaning stress and intestinal health of piglets: a review. *Frontiers in Immunology*, **13**: 1042778.

Topham NJ, Hewitt EW. 2009. Natural killer cell cytotoxicity: how do they pull the trigger?. *Immunology*, **128**(1): 7−15.

Tunçer S, Sade-Memişoğlu A, Keşküş AG, et al. 2020. Enhanced expression of HNF4αduring intestinal epithelial differentiation is involved in the activation of ER stress. *The FEBS Journal*, **287**(12): 2504−2523.

Van de Sande B, Flerin C, Davie K, et al. 2020. A scalable SCENIC workflow for single-cell gene regulatory network analysis. *Nature Protocols*, **15**(7): 2247−2276.

van der Flier LG, Haegebarth A, Stange DE, et al. 2009. OLFM4 is a robust marker for stem cells in human intestine and marks a subset of colorectal cancer cells. *Gastroenterology*, **137**(1): 15−17.

Wan WZ, Liu Q, Lionakis MS, et al. 2015. Atypical chemokine receptor 1 deficiency reduces atherogenesis in *ApoE*- knockout mice. *Cardiovascular Research*, **106**(3): 478−487.

Wang YL, Song WL, Wang JL, et al. 2020. Single-cell transcriptome analysis reveals differential nutrient absorption functions in human intestine. *Journal of Experimental Medicine*, **217**(2): e20191130.

Wiertsema SP, van Bergenhenegouwen J, Garssen J, et al. 2021. The Interplay between the gut microbiome and the immune system in the context of infectious diseases throughout life and the role of nutrition in optimizing treatment strategies. *Nutrients*, **13**(3): 886.

Wolf FA, Hamey FK, Plass M, et al. 2019. PAGA: graph abstraction reconciles clustering with trajectory inference through a topology preserving map of single cells. *Genome Biology*, **20**(1): 59.

Yang L, Yang HY, Chu YX, et al. 2021. CREPT is required for murine stem cell maintenance during intestinal regeneration. *Nature Communications*, **12**(1): 270.

Yao YC, Yao JY, Boström KI. 2019. SOX transcription factors in endothelial differentiation and endothelial-mesenchymal transitions. *Frontiers in Cardiovascular Medicine*, **6**: 30.

Zhang MM, Wu CC. 2020. The relationship between intestinal goblet cells and the immune response. *Bioscience Reports*, **40**(10): BSR20201471.

Zheng L, Duarte ME, Sevarolli Loftus A, et al. 2021. Intestinal health of pigs upon weaning: challenges and nutritional intervention. *Frontiers in Veterinary Science*, **8**: 628258.

Zhu YL, Zhou ZM, Huang T, et al. 2022. Mapping and analysis of a spatiotemporal H3K27ac and gene expression spectrum in pigs. *Science China Life Sciences*, **65**(8): 1517−1534.

Zorn AM, Wells JM. 2009. Vertebrate endoderm development and organ formation. *Annual Review of Cell and Developmental Biology*, **25**: 221−251.